IEEE Access
Multidisciplinary ⋮ Rapid Review ⋮ Open Access Journal

Received 29 January 2025, accepted 27 February 2025, date of publication 5 March 2025, date of current version 28 March 2025.

Digital Object Identifier 10.1109/ACCESS.2025.3548311

RESEARCH ARTICLE

Reconfigurable and Highly-Miniaturized Low-Noise Amplifiers Based on Tunable Filtering Loads

ANDRÉS FONTANA[1], (Member, IEEE),
STEVEN MATTHEW CHENG[1,2], (Graduate Student Member, IEEE),
AND DIMITRA PSYCHOGIOU[1,2], (Senior Member, IEEE)
[1]Advanced RF Technology Group, Tyndall National Institute, Cork 021, T12R5CP Ireland
[2]School of Engineering, University College Cork, Cork 021, T12K8AF Ireland

Corresponding author: Andrés Fontana (andres.fontana@tyndall.ie)

This work was supported by the Research Ireland (RI) under Grant 20/RP/8334 and Grant 13/RC/2077_P2.

ABSTRACT This article reports on new types of reconfigurable and multifunctional low-noise amplifier filters (LNAF) for sub-6 GHz New Radio (NR) S-band applications. The proposed LNAF concepts are based on complex-terminated bandpass filter (BPF)-type output matching networks that facilitate quasi-elliptic transfer functions that can be tuned in terms of bandwidth (BW), center frequency (f_{cen}), and can be intrinsically switched-off. To validate the proposed approaches, four proof-of-concept LNAF prototypes were realized by means of static and varactor-loaded microstrip resonators. Further size reduction is introduced in one of the prototypes through a co-designed filtering-based LNAF using tapped line resonators. For practical validation purposes, four alternative prototypes, namely LNAF I-IV, were manufactured and tested. They exhibit the following features: i) LNAF I: passband mode with f_{cen} tuning: 2.64-3.25 GHz, fractional bandwidth (FBW) tuning: 11.9-31.6% (2.65:1), gain: 16.5 dB, noise figure (NF) $<$ 0.86 dB, third order output intercept point (OIP3): 10.87 dBm, and an intrinsically switched-off mode with isolation $>$ 39 dB; ii) LNAF II: passband mode with f_{cen} tuning: 3.61-3.82 GHz, FBW: 6.3%, gain: 10.2-12.6 dB, NF $<$ 0.95 dB, OIP3 $>$ 11.15 dB, and an intrinsically switched-off mode with isolation $>$ 37.07 dB; iii) LNAF III: passband mode with f_{cen}: 3.99 GHz, FBW: 6.48%, gain: 14.3 dB, NF $<$ 1.1 dB, OIP3 $>$ 13.2 dB, and footprint reduction of 49% with respect to LNAF II. A 2-stage LNAF prototype, named LNAF IV, is implemented to achieve higher gain of 22.6 dB and NF $<$ 1.1 dB at 3.98 GHz with 15% less area than LNAF II.

INDEX TERMS Bandwidth tuning, center frequency tuning, co-design, low-noise amplifier, reconfigurable LNA, filter LNA, tunable filter.

I. INTRODUCTION

Global 5G deployments have resulted in an increasing number of communication channels for commercial use within the sub-6 GHz spectrum [1], [2]. Specifically, frequencies in the S- and C-bands are being allocated differently across the world. For example, mobile operators in Australia and South Korea have adopted the 3.4-3.7 GHz and 3.7-4.0 GHz bands, Canada utilizes the 3.475-3.65 GHz and the 3.65-4.0 GHz bands, whereas Europe employs the 3.4-3.8 GHz range, and the United States of America uses frequencies between 3.1-3.45 GHz, 3.45-3.55 GHz, 3.55-3.7 GHz, and 3.7-3.98 GHz [3], [4]. As such, to facilitate global connectivity, multi-standard and multifunctional RF front ends (RFFEs) need to be incorporated in the RF transceivers of modern communication systems to facilitate seamless connectivity. Additionally, emerging RFFEs would need to support even higher data rates, lower latency, and wider bandwidths (BWs) than what is possible today while having the smallest possible energy and footprint [5], [6].

The associate editor coordinating the review of this manuscript and approving it for publication was Prakasam Periasamy.

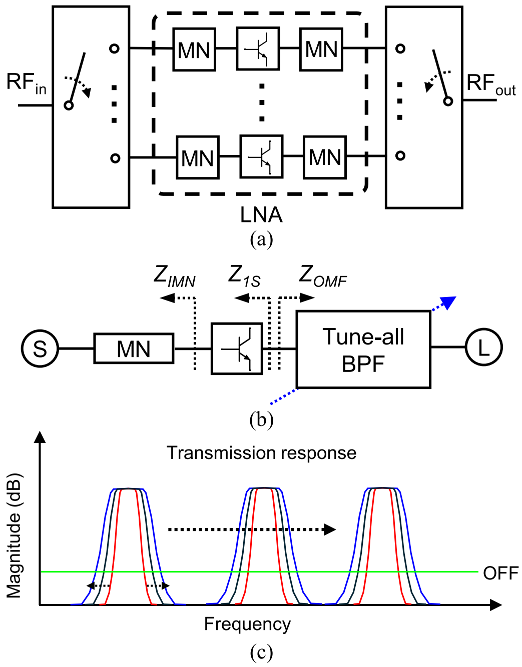

FIGURE 1. (a) Conventional architecture of a reconfigurable LNA comprising multiple RF-switched LNAs. Each LNA consists of a transistor that is matched by an input and output matching network (MN). (b) Proposed reconfigurable and multifunctional LNA filter (LNAF) based on a tunable bandpass filtering load. (c) Conceptual response of the proposed LNAF.

As such, their RFFEs would need to be highly-adaptable to facilitate re-usability of RF hardware as well as operability in changing communication environments. In this context, their bandpass filters (BPF) and their low-noise amplifiers (LNAs) need to be reconfigurable while fulfilling stringent performance requirements in terms of insertion loss, selectivity, gain and noise figure (NF) to avoid desensitizing their receivers [7].

To address these technological challenges, recent research efforts are increasingly geared towards the realization of highly-reconfigurable LNAs [8], [9], [10], [11], [12], [13], [14], [15], [16], [17], [18], [19] and BPFs with multiple levels of tunability [20], [21], [22], [23], [24], [25], [26], [27], [28], [29], [30]. RF-switched LNA banks comprising multiple narrowband in-parallel cascaded LNAs are the most straightforward method to reconfigure an LNA, as shown in Fig. 1(a) [8], [31]. However, this method leads to RFFEs with large footprints and complexity due to requiring a dedicated LNA module for each frequency band. Furthermore, the NF is compromised by the loss of the switches used for selecting the channel. To reduce the switch count—$2N$ for operation in N bands—switchless configurations [9], [10], [11], where reconfigurability is achieved by modifying the transistor's bias can be explored. In [9] the LNA's center frequency is tuned between 21 GHz and 32.5 GHz with a NF between 1-1.2 dB. Another switchless approach is presented in [10] to tune the f_{cen} of the LNA between 39 GHz and 48 GHz with NF of 3.9-4.8 dB. In yet another approach, a switched matching network (MN) is used [12], reducing the number of active components in the RFFE. This method exhibits multi-band switching between 24 GHz, 28 GHz and 39 GHz with NF between 4.5-5.5 dB. However, these approaches ([9], [10], [11], [12]) only support discrete reconfigurability.

For analog tuning, continuously tunable matching networks can be implemented at either the input [13] or output [14] of the LNA. In particular, the reconfigurable LNA concept in [13] showcased continuous frequency tuning from 1.9-2.4 GHz with NF between 3.2-3.7 dB. In [14], analog f_{cen} tunability between 28-39 GHz was demonstrated with NF between 2.4-2.8 dB. Although these LNA approaches functionalize continuously tunable bands, their selectivity is poor; thus, requiring additional filtering to be added in the RFFE. Further reconfigurability is shown in passive BPFs. In [23], a reconfigurable broadband single-/dual-band and narrowband dual-band BPF is reported by loading cross type resonators and parallel stubs. In [26], a reconfigurable wideband-to-tri-band BPF is introduced by combining open and short loaded stub resonators. Both demonstrations exhibit reconfiguration to predetermined frequency bands as a consequence of the use of p-i-n diode switches. A reconfigurable bandpass-to-bandstop filter controlled by a single p-i-n diode switch is reported in [28]. This approach is also combined with varactor diodes to achieve center frequency tuning. Multiple levels of BPF transfer functions with continuous tunability are presented in [20], where a five-pole/four-transmission zero (TZ) prototype is shown featuring f_{cen} and BW reconfigurability, in addition to a switch-off state.

Selectivity enhancement in the receiver chain of the RFFE is conventionally implemented by cascading BPFs with LNAs. However, this approach leads to large size and low signal-to-noise ratio (SNR) due to the need for inter-stage MNs. As a consequence, co-designed LNA filters (LNAFs) are increasingly considered to eliminate the need for MNs [15]. Co-designed filtering-power amplification concepts have also been shown in [32] and [33] however for static component implementation and using bulky substrate integrated waveguide (SIW) based loads in [32] and bulky air-filled waveguide cavities in [33]. Unlike conventional 50-ohm MNs, co-designed BPFs are used to match the complex impedance terminations of LNAs, performing the role of compact frequency selective matching networks directly integrated into the transistor's port. Such a concept has been applied to the realization of LNAs with filtering capabilities; the so called LNAF concept. An example of this approach is presented in the LNAF in [16], demonstrating a frequency tuning between 2.8 GHz and 4 GHz, NF ranging from 3.4 dB to 4.6 dB, and gain between 16.7 dB and 14.2 dB. However, its frequency selectivity is relatively low due to the use of single-resonator MNs. In [34], a reconfigurable multimode LNAF with single, concurrent dual-band, and intrinsic switch-off operation is reported. This work is based on a coupling matrix co-design methodology for developing complex-matched BPFs. However, the prototypes in [34] are static or exhibit a very limited degree of tunability in terms of center frequency, in addition to relatively high NF and large footprint as a result of the use of half-wavelength BPFs.

Considering the aforementioned limitations and the need for fully-reconfigurable and highly-miniaturized LNAs with high frequency selectivity, this manuscript reports on new design and practical implementation concepts to realize compact fully-reconfigurable and multifunctional LNAFs. The proposed concepts are based on complex-terminated fully-reconfigurable BPFs serving as output matching networks (OMNs), facilitating unique operational characteristics such as low-noise amplification, frequency selectivity, and transfer function that can be simultaneously tuned in terms of f_{cen}, BW, and it can also be intrinsically switched-off. Specifically, this work discusses two tunable BPF-based MNs (i.e., BPF I, II) with intrinsic switching-off capability. The BPF I-based MN topology features a fully-reconfigurable transfer function that allows simultaneous tuning of f_{cen} and BW, extending the tuning capabilities of previous reported LNAF concept [34], and greatly reducing the NF without affecting the gain. The BPF II-based MN configuration is designed to select between two adjacent bands (e.g., 3.4-3.7 GHz and 3.7-4 GHz) taking advantage of mixed coupling techniques and quarter-wavelength resonators implementing the fewest possible reconfigurable elements. An alternative method to miniaturize the size of the LNAF by incorporating DC biasing at the resonator is also introduced based on the latter topology exhibiting 15% less area. Furthermore, it demonstrates scalability to LNAFs with higher gain, higher selectivity, and has minimum impact on the NF by using a cascaded LNAF approach.

The content of this manuscript is organized as follows. Section II presents the operating principles of BPF I and BPF II. The LNAFs design methodology is discussed in Section III. Section IV presents the experimental validation of the concepts through the design and testing of four prototypes at S-band. Finally, the contributions of this work are outlined in Section V.

II. RECONFIGURABLE FILTER MATCHING NETWORK

The proposed LNAF concept is presented in Fig. 1(b). It comprises a low-noise transistor, an input matching network (IMN), and an OMN implemented by a tunable complex-matched BPF. Two different BPF architectures, namely BPF I and BPF II, are considered as OMNs with their coupling routing diagrams (CRD) depicted in Fig. 2(a) and (b), respectively. BPF I comprises two in-line resonators (1, 2) and a TZ generation section that is shaped by resonators 3, 4 and a non-resonating node. They combinedly result in a transfer function that is shaped by three poles and two TZs. Independent tuning of f_{cen} and BW can be obtained by varying the location of the poles and the TZs of the quasi-elliptic filter as demonstrated in [20]. In particular, the pole locations are varied by modifying the self-coupling coefficients of the resonators, demonstrating f_{cen} tuning as shown in Fig. 2(c). In terms of TZ tuning, only resonators 3 and 4 need to be altered as depicted in Fig. 2(d), facilitating

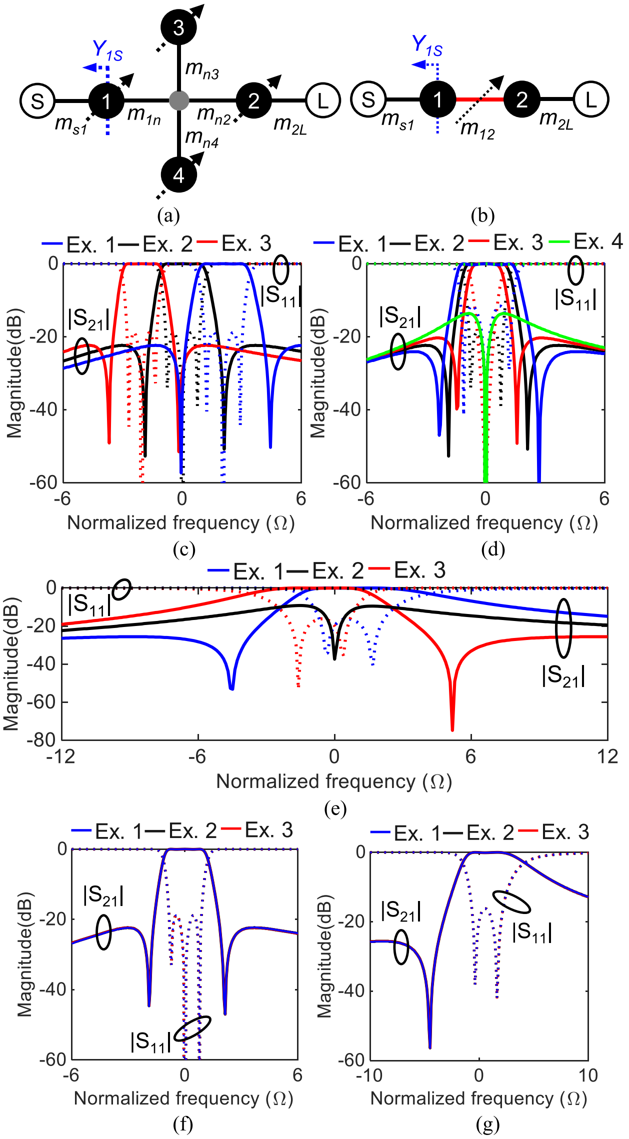

FIGURE 2. (a) CRD of the tune-all quasi-elliptic BPF I that is used as an output load of the LNA. Black circles: resonators; white circles: source and load; grey circles: non-resonating nodes; black lines: couplings. (b) CRD of a second order BPF with reconfigurable mixed coupling (BPF II) used as an output load of the LNA. Black circles: resonators; white circles: source and load; black lines: frequency-independent couplings; red line: frequency-dependent coupling. (c) Synthesized S-parameter response of the CRD in (a) when resonators 1-4 are reconfigured as follows: $m_{11}=m_{22}=-2$, 0, and 2, $m_{33}=4$, 2, and 0 and $m_{44}=0$, -2, and -4 for Examples 1, 2, and 3 respectively. (d) Synthesized S-parameter response of the CRD in (a) when resonators 3 and 4 are tuned. $m_{33}=-m_{44}=2.5$, 2, 1.5, and 0 for Examples 1, 2, 3, and 4 respectively. (e) Synthesized S-parameter response of the CRD in (b) when the mixed coupling m_{12} is altered between 1.65+0.34Ω, 0.01+0.34Ω, and 1.65-0.34Ω for Examples 1, 2, and 3 respectively. (f) Synthesized response of BPF I for different source loads: $Z_s=55$-j10 Ω, 50 Ω, and 35+j40 Ω for Examples 1, 2, and 3 respectively. For all BPF I examples, $m_{s1}=m_{2L}=1.22$, $m_{12}=1.65+0.34$Ω, and $m_{11}=m_{22}=0$. For all BPF I examples, $m_{s1}=m_{2L}=1.05$, $m_{1n}=m_{n2}=1.45$, $m_{n3}=m_{n4}=2$, $m_{11}=m_{22}=0$, $m_{33}=-m_{44}=2$ unless stated otherwise. (g) Synthesized response for BPF II for different source loads: $Z_s=55$-j10 Ω, 50 Ω, and 35+j40 Ω for Examples 1, 2, and 3 respectively.

BW reconfigurability and an intrinsically switched-off state. BPF II exhibits a two-pole/one TZ transfer function that is obtained by coupling two in-line resonators (1, 2) [35] with a

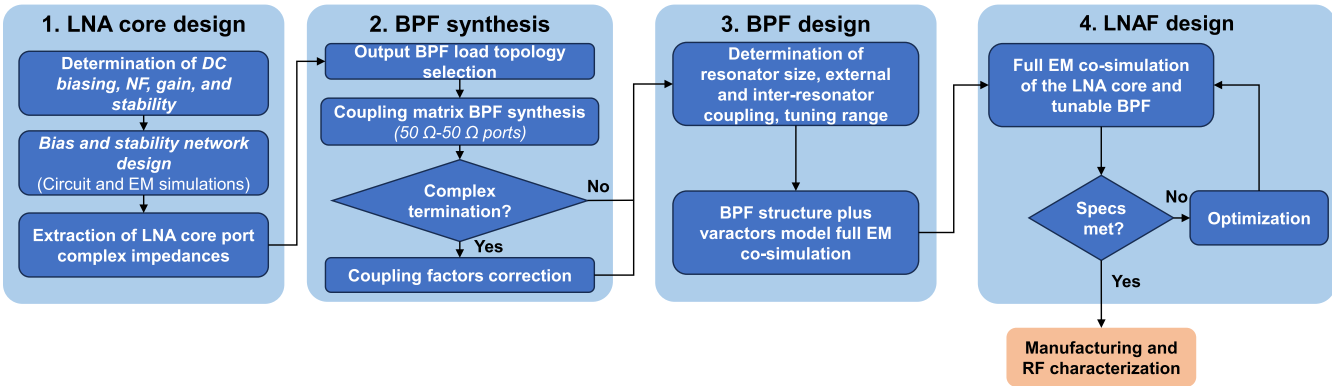

FIGURE 3. Reconfigurable LNAF design flow chart.

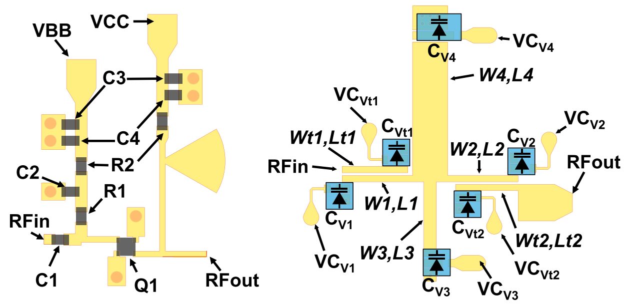

(a) (b)

FIGURE 4. (a) LNA core including DC bias and stability network: Q1: BFP840FESD, C1 = 47 pF (GQM1885C1H470JB01J), C2 = 39 pF (GQM1885C1H390JB01J), C3 = 2.2 μF, C4 = 0.22 uF, R1 = 15 kΩ, R2 = 50 Ω. (b) Layout of BPF I: W1=W2=Wt1=Wt2=0.8 mm, W3=1.6 mm, W4=4.5 mm, L1=L2=9 mm, L3=9.5 mm, L4=17 mm, Lt1=Lt2=8.4 mm, Cv1 to Cv6: MAVR000120.

frequency-dependent element that can be implemented by a mixed coupled inter-resonator coupling element [36]. In this case, f_{cen} is reconfigured by varying the mixed coupling, instead of conventionally tuning the resonators to reduce the number of tuning elements, however at the expense of limited tunability. An intrinsic switch-off mode of operation is also obtained by making the mixed coupling equal to zero [37], [38] as shown in Fig. 2(e) when BPF II is terminated to 50 Ω loads.

To match the LNA transistor using BPFs as OMNs, the coupling matrix must be modified such that its input/output impedance becomes complex. Specifically, the external coupling for the in-line resonator close to the complex termination m_{S1} needs to be altered as also discussed in [39]. Considering the CRD in Fig. 2(a) and (b), $Y_{1S} = Z_{1S}^{-1}$ is the admittance seen by resonator 1 when the source is terminated to 50 Ω as in (1) and Y'_{1S} is the admittance seen by resonator 1 when the source is terminated to an arbitrary complex impedance Z_S=$(R+jX)$ Ω as in (2). Then, to maintain the same transfer function, Y'_{1S} must be equal to Y_{1S}. This can be achieved by adding a reactance B and by modifying the coupling coefficient to m'_{S1} as described in (3) and subsequently setting (1) equal to (3). As a result, the coupling coefficients can be calculated using (4) and (5). In particular, the real part of the complex termination is compensated by the external coupling coefficient m'_{S1} as in (4) while the imaginary part of the complex termination is matched by modifying the additional reactance B as in (5). To illustrate the effectiveness of the design method, Fig. 2(f) and (g) show the S-parameter response of BPF I and II for arbitrary complex terminations of (55-j10) Ω and (35+j40) Ω for Examples 1 and 3, respectively. As observed, the transfer function of the complex-matched BPFs is the same as the one obtained by the conventional 50 Ω-terminated BPFs successfully validating the proposed design method.

$$Y_{1S} = (m_{S1})^2 \cdot Z_o \tag{1}$$

$$Y'_{1S} = (m_{S1})^2 \cdot (R + jX) \tag{2}$$

$$Y'_{1S} = \left(m'_{S1}\right)^2 \cdot (R + jX) + jB \tag{3}$$

$$m'_{S1} = m_{S1} \cdot \sqrt{Z_o/R} \tag{4}$$

$$B = -X \cdot \left(m'_{S1}\right)^2 \tag{5}$$

III. LNA DESIGNS

A. LNA CORE DESIGN

The design steps of the proposed devices are described in the flow chart depicted in Fig. 3. Specifically, the LNA design starts by defining its core and its bias network (step 1 in Fig. 3). A discrete RF heterojunction bipolar transistor (HBT) BFP840FESD from Infineon is chosen as a low-noise amplifier for the designs presented in this article. This device features a minimum noise figure NFmin@$_{5.5\text{ GHz}}$ = 0.75 dB, that is suitable for Frequency Range 1 (FR1) low voltage applications. The LNA is set in a common emitter configuration with emitter degeneration to improve the transistor's input impedance, NF, and gain performance [40]. As illustrated in Fig. 4(a), the transistor is biased using two independent power supplies ($VBB = 1.1$ V, VCC=2.1 V, $IC =$ 5 mA) through an RF choke and a base resistance R_1. Stability resistors R_2 are also added in the DC bias paths to facilitate unconditional stability. To match the LNA for a specific NF and/or gain, the constant gain and noise circles need to be plotted for the desired design f_{cen} of operation so that its input and output impedances can be selected for optimal NF or gain or a compromise between these two as shown in Fig. 5.

B. BPF SYNTHESIS AND LNAF I DESIGN

The first prototype, LNAF I, demonstrates the application of BPF I as an OMN to functionalize an agile multifunctional LNAF with tune-all reconfigurability. The LNAF was designed for $f_{cen} = 2.85$ GHz using as a reference its constant gain (red) and noise circles (blue) in Fig. 5(a). A $Z_{IMN} = (66.9+j19.3)\ \Omega$ and $Z_{OMF} = (54.8+j9.8)\ \Omega$ were selected for NF = 0.75 dB and gain=16.4 dB as part of the last task of step 1 in Fig. 3. Its IMN is conventionally designed using a shunt and series stub approach leading to an RL > 10 dB from 1.9-4.45 GHz. Its output is conjugately matched to $Z_{1S} = Z^*_{OMF}$ using a complex-matched BPF I-based OMN with FBW=12%. Figure 4(b) depicts the layout of the continuously tunable OMN using as a basis the CRD values in the caption of Fig. 2 and $m'_{s1} = 1$ and $m'_{11} = 0.2$ obtained by (1)-(5) (step 2 in Fig. 3). It was implemented by microstrip type capacitively-loaded resonators terminated to varactors C_{Vi}, with $i = 1$ to 4 (step 3 in Fig. 3). Its dimensions and utilized SMD component characteristics are provided in the caption of Fig. 4 (step 4 in Fig. 3). Considering that Z_{IMN} and Z_{1S} are frequency dependent, their values within the tuning range of BPF I is illustrated in Figure 5(c). The transistor's impedance conditions along with the design specifications at the maximum and minimum operating frequency for minimum gain (16 dB at 2.65GHz and 15 dB at 3.5 GHz) and maximum NF (1 dB) at these frequencies are depicted on a Smith-chart. The intersection region determined by the gain and noise circles defines an area of Z_{IMN} values satisfying these specifications. Some Z_{IMN} impedances are marked as reference points with white circles in Fig. 5(c) to delimit the intersection region and to map an area (black circles) with their corresponding complex conjugate impedances at the drain terminal Z^*_{1S}. To ensure good matching at the drain terminal, the complex-matched BPF I-based OMN must satisfy $Z_{OMF} = Z^*_{1S}$ at every frequency. The Z_{OMF} area highlighted in blue in Fig. 5(c) exhibits all the possible values that can be achieved with the BPF I load shown in Fig. 4(b) when the varactors C_{V1} to C_{V6} are tuned. As observed, the Z_{OMF} area completely covers all the desired Z^*_{1S} impedances, thus demonstrating the potential to accomplish the minimum design specifications.

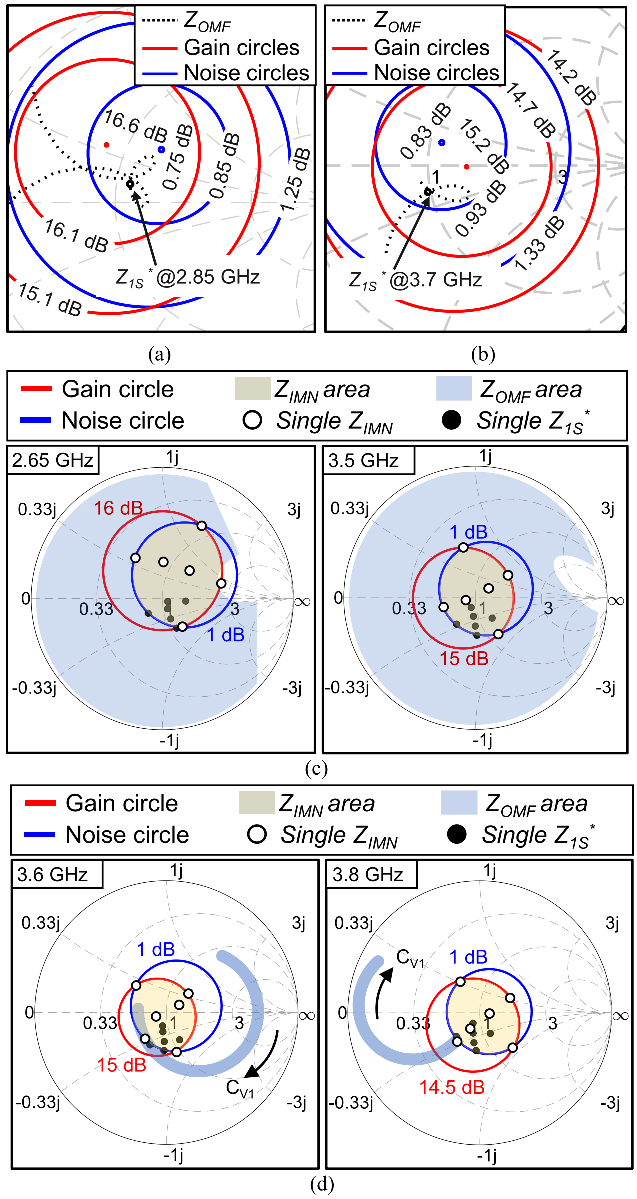

FIGURE 5. Constant gain and noise circles of the transistor plotted on a Smith-chart alongside the impedance of the output BPF MN Z_{OMF} and the required conjugate impedance Z^*_{1S}. Red circles: constant gain circles, blue circles: constant NF circles. (a) BPF I at the design frequency of 2.85 GHz. (b) BPF II at the design frequency of 3.7 GHz. (c) Realizable Z_{OMF} impedances of BPF I when the varactors C_{V1} to C_{V6} are tuned. Left: minimum tuning frequency of 2.65 GHz. Right: maximum tuning frequency of 3.5 GHz. (d) Realizable Z_{OMF} impedances of BPF II when the varactor C_{V1} is tuned. Left: minimum tuning frequency of 3.6 GHz. Right: maximum tuning frequency of 3.8 GHz. White circles: Z_{IMN} impedances within the gain and noise circles design specifications area, and Black circles: Z^*_{1S} impedances from the corresponding Z_{IMN} values.

C. BPF SYNTHESIS AND LNAF II DESIGN

The second prototype, LNAF II, demonstrates the application of BPF II. In this case BPF II has been materialized using microstrip quarter wavelength-long parallel coupled resonators (PCRs) that are directly tapped by the RF ports [41], [42]. Figure 6(a) depicts the layout of BPF II utilized as an OMN (step 3 in Fig. 3). Mixed coupling implemented by means of a tunable varactor [36], [43] is used to: i) reconfigure the filter operation between two adjacent frequency bands, ii) enhance the out-of-band isolation by introducing one TZ, and iii) to intrinsically switch-off the LNAF by making the inter-resonator coupling equal to zero. The LNAF II is designed for $f_{cen} = 3.7$ GHz (i.e, the average frequency of the tuning range: 3.6 GHz to 3.8 GHz). The corresponding constant gain (red) and noise circles (blue)

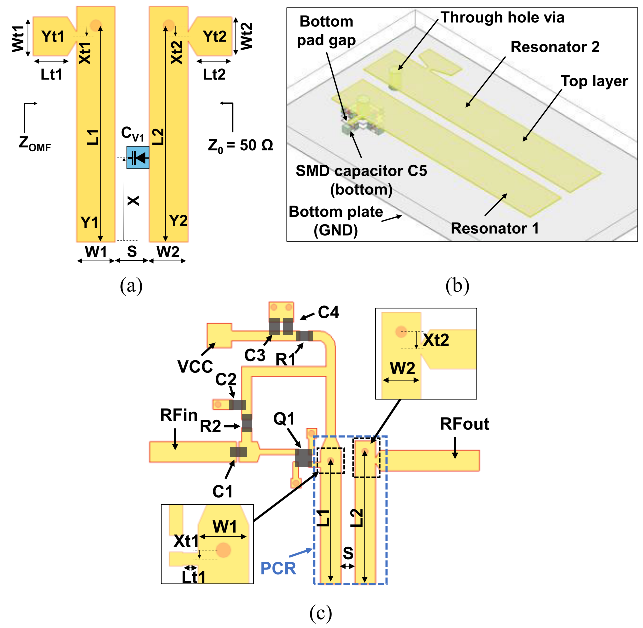

FIGURE 6. **(a) Layout of BPF II comprising two quarter-wavelength-long microstrip parallel coupled resonators (PCRs). W1=W2= 3.62 mm, Wt1=Wt2= 0.4 mm, L1=13.97 mm, L2=14.11 mm, Xt1=1.58 mm, Xt2=2.18 mm, S=1.7 mm. LNAF III and IV: W1=W2= 1.76 mm, Wt1=0.2 mm, Wt2= 1.78 mm, L1=10.17 mm, L2=10.48 mm, Xt1=1.42 mm, Xt2=1.27 mm, S=0.73 mm, Cv1: MAVR000120. (b) 3D view of the co-designed PCR-based BPF II excited by two asymmetric ports. (c) Layout of LNAF III where the components are Q1: Q2: BFP840FESD, C1 = 47 pF (CGA1A2C0G1H470J030BA), C2 = 39 pF (CBR06C390JAGAC), C3 = 0.22 μF, C4 = 200 pF, C5 = 10 pF (GJM0335C2A100GB01), R1 = 50 Ω, R2 = 62 kΩ.**

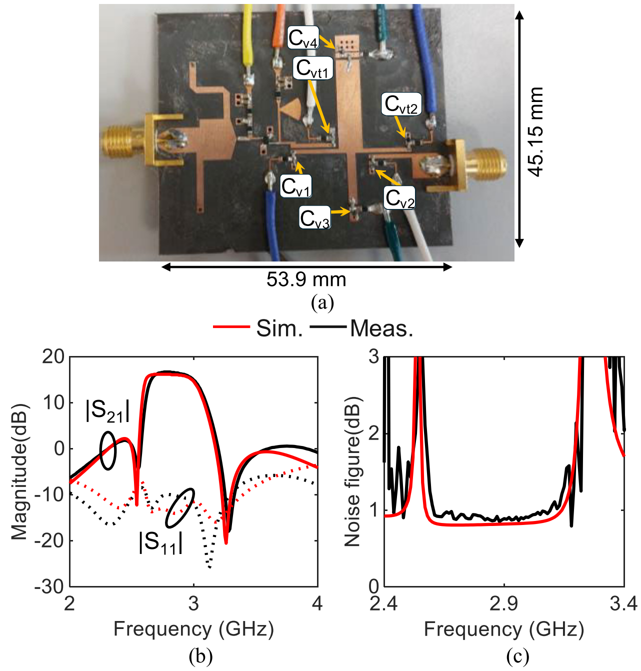

FIGURE 7. **LNAF I. (a) Manufactured prototype. (b) RF-measured and EM-simulated S-parameters for one tuning state. (c) RF-measured and EM-simulated NF for the same tuning state as in (b).**

are depicted in Fig. 5(b). A Z_{IMN} of (51.8+j4.3) Ω and a Z_{OMF} of (50-j10) Ω were chosen for NF = 0.87 dB and gain=14.7 dB (last task of step 1 in Fig. 3). On this basis, the transistor input is conventionally matched using a series stub which leads to an RL >10 dB at f_{cen}. Furthermore, it is also matched to $Z_{1S} = Z_{OMF}^{*}$. The BPF II characteristics are determined using the design methodology in Section II and for an FBW= 5%. The CRD values listed in the caption of Fig. 2 are used wherein m'_{11} is altered to −0.3 using (1)-(5) to facilitate matching to Z_{1S}, while the resonator 2 remains matched to 50 Ω (step 2 in Fig. 3). Its dimensions [44], [45] are provided in the caption of Fig. 6 (step 4 in Fig. 3). As in the previous case, the capability of the proposed BPF II-based OMN complies with the frequency-dependent Z_{IMN} and Z_{1S} impedances as illustrated in Fig. 5(d). This figure shows how the variation of Z_{OMF} when sweeping C_{V1} accomplishes the complex matching condition $Z_{OMF} = Z_{1S}^{*}$ at the maximum and minimum operating frequency for minimum gain (15 dB at 3.6 GHz and 14.5 dB at 3.8 GHz) and NF (1 dB) specifications at these frequencies.

D. BPF SYNTHESIS AND LNAF III & IV DESIGN

To further reduce the size of the LNAF using the BPF II-based OMN, BPF II can be modified to use its input resonator as part of the DC bias network of the transistor [46]. As shown in Fig. 6(b), the through-hole via placed in resonator 1 is isolated from the bottom ground by a DC isolated pad that is connected to ground through four SMD capacitors. When introducing these bypass capacitors, the physical length of resonator 1 needs to be decreased to compensate for their loading effect. No further modifications are necessary on resonator 2, thus enabling the utilization of the same bias network for the inter-resonator coupling as in the case of LNAF II. To validate the benefits of this integration scheme, a static LNAF III prototype with 49% smaller area than the one occupied by LNAF II was designed using the BPF II OMN shown in Fig. 6(b) and (c). The targeted design specifications for this case were set as follows f_{cen} of 4 GHz, gain ≥ 10 dB, 6.25% ≤ FBW ≤ 7.50%, NF ≤ 2 dB, and RL ≥ 10 dB. It is worth noting that the device was modified to be biased with sonly one power supply. The DC operating points were set as $VCC = 1.78$ V, $VBB = 0.83$ V, and $IC =$ 5 mA, resulting in a static power consumption of $P_{DC} =$ 8.9 mW. As in the previous designs, emitter degeneration was also implemented for the LNA transistor and the conjugated output impedance for this configuration was selected as $Z_{OMF} = (40 - j50)$ Ω. In this case the OMN was designed for a second order Chebyshev transfer function with FBW of 5% and 0.045 dB. The bias network is comprised of resonator 1, C_3, C_4, R_1 and R_2, while C_1, C_2 and C_5 are used as DC block and bypass capacitors. The specific dimensions and value of components used for this design are detailed in the caption of Fig. 6.

To demonstrate scalability to higher gain, transfer function selectivity and applicability of the method to cascade-based LNA configurations, a two-stage LNAF IV (based on

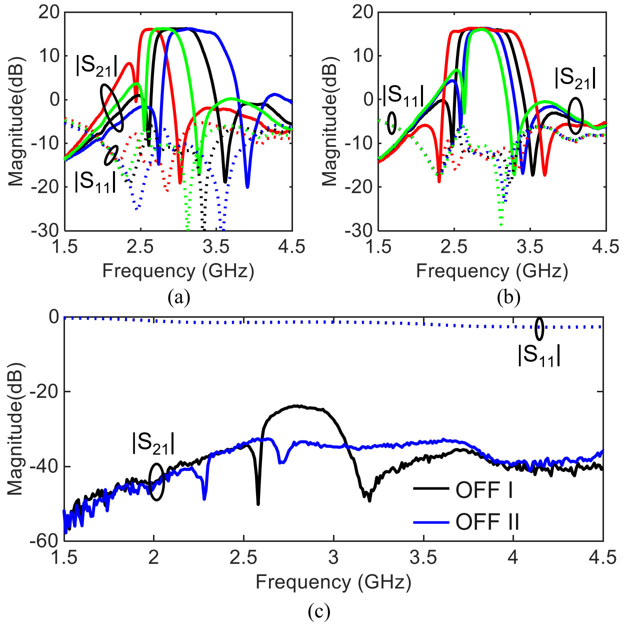

FIGURE 8. LNAF I. (a) Measured S-parameters for different f_{cen} tunable states. (b) Measured S-parameters for various tunable BW states. (c) Measured intrinsic-off states. OFF I: transistor bias removed and OFF II: transistor bias removed and the TZs are configured one above another at f_{cen}.

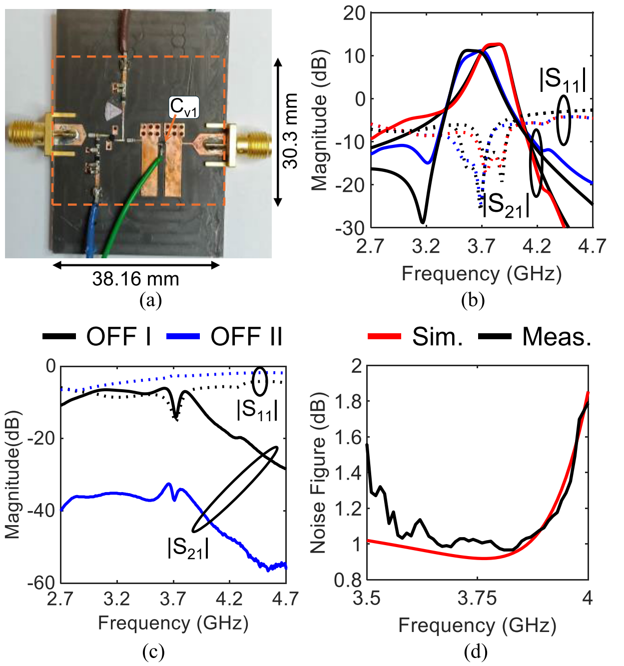

FIGURE 9. LNAF II. (a) Manufactured prototype. (b) Measured (blue and red plots) and EM-simulated (black plots) S-parameter response of tunable f_{cen} for alternative C_{V1} biasing states: $f_{cen} = 3.61$ GHz (blue), $f_{cen} = 3.82$ GHz (red). (c) Measured intrinsic-off states: OFF I: TZ tuned above f_{cen} while the transistor is on and OFF II: TZ tuned above f_{cen} while the transistor is off. (d) Measured and EM-simulated NF for $f_{cen} =$ 3.82 GHz in (b).

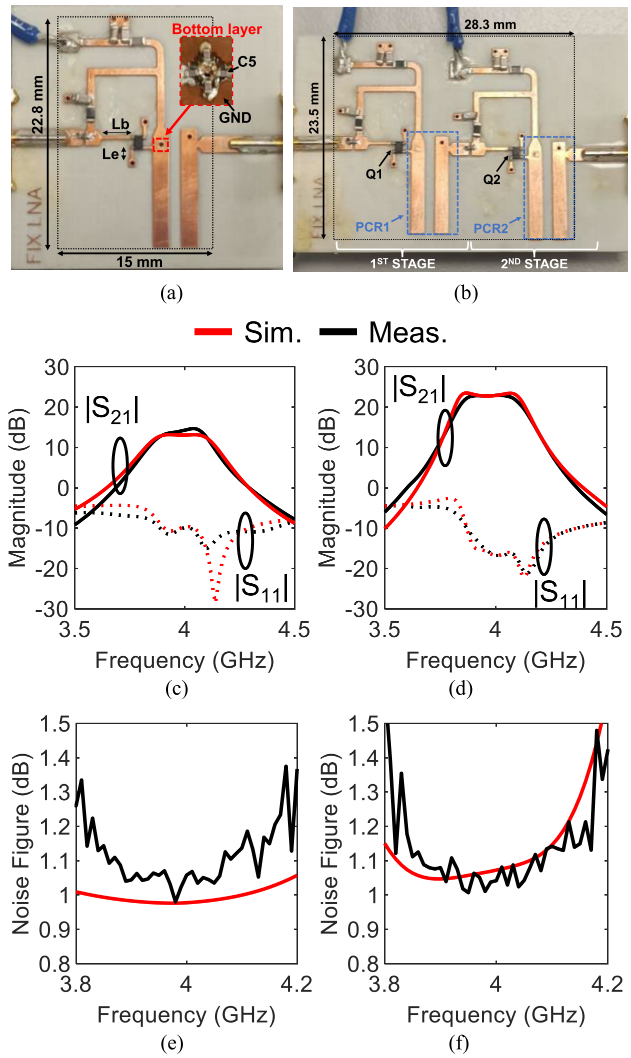

FIGURE 10. (a) Manufactured prototype of LNAF III. (b) Manufactured prototype of LNAF IV. Measured S-parameters for the: (c) LNAF III, and (d) LNAF IV. Measured noise figure for the: (e) LNAF III, and (f) LNAF IV.

two LNAF III stages) was performed without significant degradation of NF. Thanks to the higher integration of this approach, it exhibits significantly higher gain of 20 dB when compared to LNAF II while having similar NF < 2 dB and a 15% smaller size.

IV. EXPERIMENTAL VALIDATION

To validate the LNAF concept, four prototypes (LNAF I-IV) using BPF I and BPF II-based OMNs were implemented using a hybrid PCB-based integration approach. Specifically, LNAF I and II were manufactured on a low-loss RT Duroid 5880 substrate (dielectric permittivity ε_r: 2.2, board thickness: 1.57 mm, and loss tangent: 0.0009) to reduce the overall losses and NF. LNAF III and LNAF IV were implemented on a higher permittivity substrate RO4003C (dielectric permittivity ε_r: 3.55, board thickness: 0.82 mm, and loss tangent: 0.0027) for size compactness. All the prototypes were fabricated in-house, and were characterized in terms of S-parameters, gain, NF, and OIP3 by means of a Keysight PNA-X N5244A network analyzer.

TABLE 1. Comparison with state-of-the-art reconfigurable LNAs.

	Technology	Filter + Switch Function	Type of Tuning	f_{cen} (GHz)	Gain (dB)	NF (dB)	P_{DC} (mW)	FBW (%)	Size (λ_g^2)
LNAF I	**PCB**	**YES**	**Continuous**	**2.65-3.25#**	**16.5**	**0.86**	**10.5**	**11.90-31.60#**	**0.480**
LNAF II	**PCB**	**YES**	**Continuous**	**3.61/ 3.82***	**10.2-12.6**	**0.97**	**11.9**	**6.30**	**0.390**
LNAF III	**PCB**	**NO**	**Continuous**	**3.99**	**14.3**	**< 1.10**	**8.9**	**6.48**	**0.170**
LNAF IV	**PCB**	**NO**	**Continuous**	**3.98**	**22.8**	**< 1.10**	**17.8**	**7.29**	**0.330**
[34]	PCB	YES	**Continuous**	3.76	17.0	1.66	12.2	3.72-17.02	2.460
[16]	PCB	NO	Continuous	2.80-4.00#	16.7-14.2	3.40-4.60	90.0	1.80	0.830
[49]	PCB	NO	Continuous	2.00-2.50/5.00#	1.6-8/5.4	1.50/2.00	28.0	N.A.	0.330
[47]	PCB	NO	Continuous	2.30-2.50/ 4.20-4.60#	3.0-12.2/ 9.5-12.9	0.50-5.00/ 2.50-5.00	41.3	N.A.	0.730
[48]	0.13 um CMOS	NO	Continuous	1.80-2.40#	20.6-22.1	3.20-3.50	9.6	N.A.	0.052†
[13]	0.13 um CMOS	NO	Discrete	1.90-2.40#	14.0-10.0	3.20-3.70	17.0	N.A.	0.083†
[11]	55 nm CMOS	NO	Discrete	27.50/ 39.50*	23.5/ 22.9	3.30/ 4.25	19.8/ 23.6	0.27/ 0.21	0.150†
[12]	45 nm SOI	NO	Discrete	24.00/ 28.00/ 39.00*	9.5/ 12.0/ 15.5	4.50/ 4.50/ 5.50	20.7	N.A.	0.690†
[10]	0.15 um GaAs pHEMT	NO	Discrete	39.00/ 48.00*	24.3/ 18.8	3.90/ 4.80	64.7/ 61.4	N.A.	3.040†
[14]	0.1 um GaAs	NO	Continuous	26.50-41.00#	25.0-27.7	2.40-2.80	74.0	N.A.	1.600†

λg: guided wavelength, *discrete tuning, #analog tuning, †in mm² (LNAs in IC process), PCB: printed circuit board. Sw.: switch function, Filt.: filter function

A. LNAF I

Fig. 7(a) shows the manufactured prototype of LNAF I and its RF measured performance is summarized in Fig. 7(b) and (c). Based on the approach introduced in [34], the OMN of the LNAF I is implemented by coupled-line and stub-loaded resonators, in such a way that the DC blocking functionality is integrated within the BPF. Its RF measured characteristics can be summarized as follows: gain = 16.5 dB, NF = 0.86 dB, 3-dB FBW = 14%, RL ≥ 10 dB, and OIP3 = 10.87 dBm. A comparison with the EM simulated performance is shown in the same figure, successfully validating the proposed concept. The tunable measured characteristics of LNAF I are provided in Fig. 8. Specifically, Fig. 8(a) demonstrates a continuously tunable passband between 2.65 to 3.25 GHz. The continuously tunable FBW capabilities of LNAF I are demonstrated in Fig. 8(b), where its FBW is continiously tuned between 11.9-31.6%. The intrinsic switch-off operation is provided in Fig. 8(c) by: i) turning off the transistor bias leading to an isolation higher than 24.7 dB and ii) by turning off the transistor and by tuning the TZs on top of the passband which further enhances the isolation to 39 dB.

B. LNAF II

The manufactured prototype of LNAF II is shown in Fig. 9(a) and its RF measured reconfigurable states are presented in Fig. 9(b) and (c). Specifically, f_{cen} is reconfigured between two adjacent bands centered at 3.61 GHz and 3.82 GHz, while maintaining an FBW of 6.3%. The measured RF characteristics for the passband centered at 3.82 GHz can be summarized as follows: gain= 12.6 dB, NF= 0.97 dB, 3-dB FBW= 6.3%, RL > 10 dB, and OIP3= 11.15 dBm. A comparison with its corresponding EM co-simulated state is also shown in Fig. 9(b), demonstrating a fairly good agreement with the experimental results. Its transfer function can be additionally intrinsically switched-off by: i) tuning the mixed coupling ($m_{12} = 0$) such that the TZ suppresses the passband with an isolation of 12.96 dB at 3.71 GHz, and ii) by turning off the transistor bias and tuning the TZ to the design frequency leading to improved isolation of 37.07 dB.

C. LNAF III

A LNAF III sample was fabricated and characterized to validate the OMN integration approach proposed in Section III. The manufactured device is exhibited in Fig. 10(a), where the inclusion of the four bottom layer capacitors C5 is displayed in the figure inset. Measured results in Fig. 10(c) and (e) for a LNAF III plotted sample centered at 3.99 GHz show: gain=14.3 dB, NF < 1.1 dB, 3-dB FBW = 6.48%, RL ≥ 10 dB, and OIP3 = 13.2 dBm. The overall area is 0.17 λg^2 versus the 0.39 λg^2 observed in LNAF II. Comparisons with EM simulations exhibit a good agreement with S-parameters and NF, demonstrating the fulfilment of the design specifications expected for this compact prototype.

D. LNAF IV

To validate the scalability of the LNAF concept and its potential for cascaded LNA approaches with higher gain and higher transfer function selectivity, LNAF IV was manufactured and measured. Its prototype is illustrated in Fig. 10(b) and its RF-measured and simulated S-parameters and NF are plotted in Fig. 10(d) and (f), demonstrating the following RF measured performance characteristics: gain =22.8 dB, 3-dB FBW=7.29 %, RL ≥ 10 dB, and NF < 1.1 dB.

To demonstrate the potential of the proposed reconfigurable LNAF approach, Table 1 compares LNAF I-IV with state-of-the-art (SOA) reconfigurable LNAs in PCB and MMIC technologies. As evidenced, the proposed approach uniquely demonstrates the potential to realize a highly-reconfigurable LNA with: i) reconfigurable filtering and high switching-off capability: ii) fully-tunable f_{cen} and BW; iii) enhanced out-of-band response; and iv) low power consumption. The characterized prototypes demonstrate a minimum gain of 10.2 dB, 14.3 dB, 16.5 dB, and 22.5 dB for LNAF I-IV, respectively, showing a performance compliant to SOA single- [10], [12], [16], [34], [47] and multi-stage [10], [11], [48] LNAs. In contrast to [34] which presented larger size, higher NF and limited reconfigurability, LNAF I and II demonstrate reconfigurable filtering loads capable of frequency dependent matching which resulted in an increased degree of tunability, lower NF and reduced footprint. Thus, enabling multi-standard operation of modern communication receivers. The proposed configurations LNAF I-IV also exhibit compact size comparable to the smallest PCB designs reported in the literature [42] operating at the L- and S-band. It should be mentioned that besides its tune-all capability and unlike the designs in Table 1, LNAF I can maintain a constant gain of 16.5 dB across the entire tuning range. The implementation of the co-integrated methodology in LNAF III and LNAF IV demonstrates a significant footprint miniaturization of 49% and 15% when compared to LNAF II with a small NF degradation. The obtained NF is quite low and comparable to the best cases among reconfigurable LNAs implemented using PCB technologies [34], [47], [49], and among the lowest power consumption devices [11], [12], [34], [48].

V. CONCLUSION

New classes of compact reconfigurable and multifunctional LNAFs with enhanced NF and capable of re-adapting their operation to sub-6 GHz New Radio (NR) S-band applications were reported. They are based on complex-matched bandpass filter BPF-type OMNs that facilitate quasi-elliptic transfer functions that can be tuned in terms of BW, f_{cen}, and can be additionally intrinsically switched-off. For practical validation purposes four alternative microstrip prototypes, namely LNAF I-IV, were manufactured and tested. They exhibit the following features: i) LNAF I: passband mode with f_{cen} tuning: 2.64-3.25 GHz, fractional bandwidth (FBW) tuning: 11.9-31.6% (2.65:1), gain: 16.5 dB, NF < 0.86 dB, third order output intercept point (OIP3): 10.87 dBm and an intrinsically switched-off mode with isolation > 39 dB; ii) LNAF II: passband mode with f_{cen} tuning: 3.61-3.82 GHz, gain: 10.2-12.6 dB, NF < 0.95 dB, OIP3 > 11.15 dB and an intrinsically switched-off mode with isolation >37.07 dB; iii) LNAF III: passband mode with f_{cen}: 3.99 GHz, gain: 14.3 dB, NF < 1.1 dB, OIP3 > 13.2 dB, and footprint reduction of 49% with respect to LNAF II. A 2-stage LNAF III prototype, named LNAF IV, is implemented to achieve a higher gain of 22.6 dB and NF < 1.1 dB at 3.98 GHz with 15% less area than LNAF II. Finally, the microstrip implementation of the proposed approaches enables the utilization of such devices not only on PCB, but also in advanced integration technologies such as low temperature cofired ceramics (LTCC), or monolithic microwave integrated circuits (MMICs), suitable for diverse 6G communication applications.

ACKNOWLEDGMENT

(Andrés Fontana and Steven Cheng contributed equally to this work).

REFERENCES

[1] I. Ahmed, M. Z. Hassan, M. Haider, and K. Hasan, "Integrated cellular and cell-free communication systems toward global connectivity: Motivations, challenges, and research roadmap," *IT Prof.*, vol. 26, no. 4, pp. 29–35, Jul. 2024, doi: 10.1109/MITP.2024.3433511.

[2] M. Ghosh, "World radiocommunications conference 2023, WRC-23," *IEEE Wireless Commun.*, vol. 30, no. 6, p. 4, Dec. 2023, doi: 10.1109/MWC.2023.10355082.

[3] Qualcomm Technol. Inc., San Diego, CA, USA. (May 31, 2023). *Global 5G Spectrum Update and Innovations for Future Wireless Systems*. [Online]. Available: https://www.qualcomm.com/content/dam/qcomm-martech/dm-assets/documents/global-5g-spectrum-status-and-innovations-for-future-wireless-systems.pdf

[4] *User Equipment (UE) Radio Transmission and Reception; Part 1: Range 1 Standalone*, document TR 38.101-1, 3GPP, 2017. [Online]. Available: https://portal.3gpp.org/desktopmodules/Specifications/SpecificationDetails.aspx?specificationId=3283

[5] A. O. Watanabe, M. Ali, S. Y. B. Sayeed, R. R. Tummala, and M. R. Pulugurtha, "A review of 5G front-end systems package integration," *IEEE Trans. Compon., Packag., Manuf. Technol.*, vol. 11, no. 1, pp. 118–133, Jan. 2021, doi: 10.1109/TCPMT.2020.3041412.

[6] Y. I. A. Al-Yasir, A. M. Abdulkhaleq, N. O. Parchin, I. T. Elfergani, J. Rodriguez, J. M. Noras, R. A. Abd-Alhameed, A. Rayit, and R. Qahwaji, "Green and highly efficient MIMO transceiver system for 5G heterogenous networks," *IEEE Trans. Green Commun. Netw.*, vol. 6, no. 1, pp. 500–511, Mar. 2022, doi: 10.1109/TGCN.2021.3100399.

[7] Y. Huo, X. Dong, W. Xu, and M. Yuen, "Enabling multi-functional 5G and beyond user equipment: A survey and tutorial," *IEEE Access*, vol. 7, pp. 116975–117008, 2019, doi: 10.1109/ACCESS.2019.2936291.

[8] T.-C. Chung, C.-W. Chen, O. T. C. Chen, and R. Y. J. Tsen, "A multi-band RF front-end receiver for Bluetooth, WCDMA, and GPS applications," in *Proc. 46th Midwest Symp. Circuits Syst.*, Cairo, Egypt, 2003, pp. 1175–1178.

[9] R. Vignesh, P. Gorre, H. Song, and S. Kumar, "A K/Ka-band switchless reconfigurable 65 nm CMOS LNA based on suspended substrate coupled line," *IEEE Access*, vol. 10, pp. 33449–33464, 2022, doi: 10.1109/ACCESS.2022.3162202.

[10] B. Ko, S. Lee, W. Seo, T. Sim, S. Kim, M.-S. Kim, and J. Kim, "A 39/48 GHz switchless reconfigurable low noise amplifier using common gate and coupled-line-based diplexer," *IEEE Trans. Circuits Syst. II, Exp. Briefs*, vol. 70, no. 11, pp. 4028–4032, Nov. 2023, doi: 10.1109/TCSII.2023.3286824.

[11] B. Liu, F. Meng, Z. Ma, K. S. Yeo, and K. Ma, "A 28/39 GHz tri-mode frequency-reconfigurable LNA for multiband 5G communications," *IEEE Trans. Circuits Syst. II, Exp. Briefs*, vol. 71, no. 9, pp. 4036–4040, Sep. 2024, doi: 10.1109/TCSII.2024.3379230.

[12] R. A. Shaheen, T. Rahkonen, and A. Pärssinen, "Millimeter-wave frequency reconfigurable low noise amplifiers for 5G," *IEEE Trans. Circuits Syst. II, Exp. Briefs*, vol. 68, no. 2, pp. 642–646, Feb. 2021, doi: 10.1109/TCSII.2020.3014571.

[13] M. El-Nozahi, E. Sanchez-Sinencio, and K. Entesari, "A CMOS low-noise amplifier with reconfigurable input matching network," *IEEE Trans. Microw. Theory Techn.*, vol. 57, no. 5, pp. 1054–1062, May 2009, doi: 10.1109/TMTT.2009.2017249.

[14] Z. Wang, D. Hou, P. Zhou, H. Li, Z. Li, J. Chen, and W. Hong, "A Ka-band switchable LNA with 2.4-dB NF employing a varactor-based tunable network," *IEEE Microw. Wireless Compon. Lett.*, vol. 31, no. 4, pp. 385–388, Apr. 2021, doi: 10.1109/LMWC.2021.3059655.

[15] Y. Gao, X. Shang, L. Li, C. Guo, and Y. Wang, "Integrated filter–amplifiers: A comprehensive review," *IEEE Microw. Mag.*, vol. 23, no. 6, pp. 57–75, Jun. 2022, doi: 10.1109/MMM.2022.3155034.

[16] M. F. Hagag, M. Abu Khater, and D. Peroulis, "Balanced-balanced tunable filtering LNA using evanescent-mode resonators," in *IEEE MTT-S Int. Microw. Symp. Dig.*, Boston, MA, USA, Jun. 2019, pp. 13–16.

[17] D. Cheng, X. Chen, Q. Chen, X. Ma, and L. Li, "A reconfigurable LNA with compact magnetic-capacitive coupling transformer networks for 5G 28-/39-GHz applications," *IEEE Microw. Wireless Technol. Lett.*, vol. 34, no. 7, pp. 915–918, Jul. 2024, doi: 10.1109/LMWT.2024.3403862.

[18] C. Xie, Z. Yu, and C. Tan, "An X/Ku dual-band switch-free reconfigurable GaAs LNA MMIC based on coupled line," *IEEE Access*, vol. 8, pp. 160070–160077, 2020, doi: 10.1109/ACCESS.2020.3020396.

[19] H.-H. Chen and Z.-M. Tsai, "Ka-/K-band frequency-reconfigurable single-input differential-output low-noise amplifier for 5G applications," *IEEE Microw. Wireless Technol. Lett.*, vol. 33, no. 9, pp. 1297–1300, Sep. 2023, doi: 10.1109/LMWT.2023.3288625.

[20] D. Psychogiou and M. Deng, "High-order coaxial bandpass filters with multiple levels of transfer function tunability," *IEEE Microw. Wireless Compon. Lett.*, vol. 30, no. 4, pp. 367–370, Apr. 2020, doi: 10.1109/LMWC.2020.2973546.

[21] D. Simpson and D. Psychogiou, "High-order and tunable balanced bandpass filters using mixed technology resonators," *Int. J. Microw. Wireless Technol.*, vol. 13, no. 7, pp. 673–681, Apr. 2021, doi: 10.1017/s1759078721000453.

[22] D. Psychogiou and R. Gómez-García, "Multi-mode-cavity-resonator-based bandpass filters with multiple levels of transfer-function adaptivity," *IEEE Access*, vol. 7, pp. 24759–24765, 2019, doi: 10.1109/ACCESS.2019.2900059.

[23] M. Wang, G. Liu, Y. Wu, J. Zhou, and Z. Cheng, "A reconfigurable bandpass filter with multi-band switching and band shiftability," *IEEE Trans. Circuits Syst. II, Exp. Briefs*, vol. 71, no. 6, pp. 2956–2960, Jun. 2024, doi: 10.1109/TCSII.2024.3355418.

[24] A. Bandyopadhyay, P. Sarkar, and R. Ghatak, "A bandwidth reconfigurable bandpass filter for ultrawideband and wideband applications," *IEEE Trans. Circuits Syst. II, Exp. Briefs*, vol. 69, no. 6, pp. 2747–2751, Jun. 2022, doi: 10.1109/TCSII.2022.3167028.

[25] K. Zhao and D. Psychogiou, "Single-to-multi-band reconfigurable acoustic-wave-lumped-resonator bandpass filters," *IEEE Trans. Circuits Syst. II, Exp. Briefs*, vol. 69, no. 4, pp. 2066–2070, Apr. 2022, doi: 10.1109/TCSII.2021.3139008.

[26] A. Bandyopadhyay, P. Sarkar, T. Mondal, and R. Ghatak, "A dual function reconfigurable bandpass filter for wideband and tri-band operations," *IEEE Trans. Circuits Syst. II, Exp. Briefs*, vol. 68, no. 6, pp. 1892–1896, Jun. 2021, doi: 10.1109/TCSII.2020.3047873.

[27] C.-W. Tang and J.-M. Jiang, "Design of the microstrip bandpass filter with 4 band-switching modes," *IEEE Trans. Circuits Syst. II, Exp. Briefs*, vol. 70, no. 6, pp. 1926–1930, Jun. 2023, doi: 10.1109/TCSII.2022.3229105.

[28] M. Fan, K. Song, Y. Zhu, and Y. Fan, "Compact bandpass-to-bandstop reconfigurable filter with wide tuning range," *IEEE Microw. Wireless Compon. Lett.*, vol. 29, no. 3, pp. 198–200, Mar. 2019, doi: 10.1109/LMWC.2019.2892846.

[29] Z. Zhang and D. Psychogiou, "Multi-functional single/multi-band bandpass filters with co-integrated RF isolator, variable phase shifter or variable attenuator functionalities," *IEEE Trans. Circuits Syst. I, Reg. Papers*, vol. 71, no. 9, pp. 4032–4045, Sep. 2024, doi: 10.1109/TCSI.2024.3419583.

[30] A. Nadeem, S. Nikolaou, D. Psychogiou, and P. Vryonides, "Multi-functional and reconfigurable bandpass filters with continuously tunable attenuation or quasi-reflectionless behavior," *IEEE Trans. Circuits Syst. II, Exp. Briefs*, vol. 71, no. 10, pp. 4466–4470, Oct. 2024, doi: 10.1109/TCSII.2024.3398497.

[31] B. Behmanesh and S. M. Atarodi, "Active eight-path filter and LNA with wide channel bandwidth and center frequency tunability," *IEEE Trans. Microw. Theory Techn.*, vol. 65, no. 11, pp. 4715–4723, Nov. 2017, doi: 10.1109/TMTT.2017.2698466.

[32] K. Chen, J. Lee, W. J. Chappell, and D. Peroulis, "Co-design of highly efficient power amplifier and high-*Q* output bandpass filter," *IEEE Trans. Microw. Theory Techn.*, vol. 61, no. 11, pp. 3940–3950, Nov. 2013, doi: 10.1109/TMTT.2013.2284485.

[33] Y. Gao, W. Ma, D. Lu, B. Zhu, P. Jia, and M. Yu, "A coupling matrix synthesized three-dimensional filtering power amplifier," *IEEE Trans. Circuits Syst. I, Reg. Papers*, vol. 71, no. 7, pp. 3074–3085, Jul. 2024, doi: 10.1109/TCSI.2024.3352603.

[34] S. M. Cheng and D. Psychogiou, "Multimode low noise amplifier filter with tunable transfer function characteristics," *IEEE Trans. Microw. Theory Techn.*, early access, Sep. 2, 2024, doi: 10.1109/TMTT.2024.3449135.

[35] Q.-X. Chu and H. Wang, "A compact open-loop filter with mixed electric and magnetic coupling," *IEEE Trans. Microw. Theory Techn.*, vol. 56, no. 2, pp. 431–439, Feb. 2008, doi: 10.1109/TMTT.2007.914642.

[36] S. Narayana and Y. K. Singh, "Third-order tunable filter with CFBW using two quarter-wavelength resonators," *Microw. Opt. Technol. Lett.*, vol. 63, no. 9, pp. 2303–2308, May 2021, doi: 10.1002/mop.32883.

[37] X. Wang, N.-Y. Zhong, H. Li, J.-Y. Chu, H. Yang, X.-L. Yang, X.-W. Zhu, and W. Wu, "Miniaturized circular substrate integrated waveguide bandpass filter with flexible mixed coupling and wide stopband rejection," *IEEE Trans. Circuits Syst. II, Exp. Briefs*, vol. 71, no. 8, pp. 3655–3659, Aug. 2024, doi: 10.1109/TCSII.2024.3369046.

[38] Z. L. Su, B. W. Xu, S. Y. Zheng, H. W. Liu, and Y. L. Long, "High-isolation and wide-stopband SIW diplexer using mixed electric and magnetic coupling," *IEEE Trans. Circuits Syst. II, Exp. Briefs*, vol. 67, no. 1, pp. 32–36, Jan. 2020, doi: 10.1109/TCSII.2019.2903388.

[39] J. A. Estrada, S. Johannes, D. Psychogiou, and Z. Popovic, "Tunable impedance-matching filters," *IEEE Microw. Wireless Compon. Lett.*, vol. 31, no. 8, pp. 993–996, Aug. 2021, doi: 10.1109/LMWC.2021.3083184.

[40] J.-T. Son, H.-W. Choi, and C.-Y. Kim, "Sub-6 GHz LNA using two-stage SNIM with series interstage inductor based on 0.5-μm GaAs E-pHEMT technology," *IEEE Microw. Wireless Technol. Lett.*, vol. 33, no. 9, pp. 1301–1304, Sep. 2023, doi: 10.1109/LMWT.2023.3295839.

[41] F. Zhu, W. Hong, J.-X. Chen, and K. Wu, "Quarter-wavelength stepped-impedance resonator filter with mixed electric and magnetic coupling," *IEEE Microw. Wireless Compon. Lett.*, vol. 24, no. 2, pp. 90–92, Feb. 2014, doi: 10.1109/LMWC.2013.2290225.

[42] S. Zhang, L. Zhu, and R. Weerasekera, "Synthesis of inline mixed coupled quasi-elliptic bandpass filters based on $\lambda/4$ resonators," *IEEE Trans. Microw. Theory Techn.*, vol. 63, no. 10, pp. 3487–3493, Oct. 2015, doi: 10.1109/TMTT.2015.2467380.

[43] A. Zakharov, M. Ilchenko, S. Rozenko, and L. Pinchuk, "Planar bandpass filters with mixed couplings," in *Advances in Information and Communication Technology and Systems* (Lecture Notes in Networks and Systems), vol. 152. Cham, Switzerland: Springer, 2021, pp. 377–393.

[44] J.-S. Hong, "Lowpass and bandpass filters," in *Microstrip Filters for RF/Microwave Applications*, 2nd ed., Hoboken, NJ, USA: Wiley, 2011, pp. 135–141.

[45] S. Caspi and J. Adelman, "Design of combline and interdigital filters with tapped-line input," *IEEE Trans. Microw. Theory Techn.*, vol. 36, no. 4, pp. 759–763, Apr. 1988, doi: 10.1109/22.3583.

[46] J. Wang, J. Wen, P.-L. Chi, and T. Yang, "A 2.8–3.8-GHz reconfigurable GaAs low-noise amplifier with improved blocker tolerance," *IEEE Microw. Wireless Technol. Lett.*, vol. 34, no. 4, pp. 419–422, Apr. 2024, doi: 10.1109/LMWT.2024.3363715.

[47] A. Kumar and N. P. Pathak, "Reconfigurable concurrent dual-band low noise amplifier for noninvasive vital sign detection applications," in *Proc. Int. Conf. Adv. Comput., Commun. Informat. (ICACCI)*, Delhi, India, Sep. 2014, pp. 2496–2500.

[48] A. Slimane, F. Haddad, S. Bourdel, S. A. Tedjini-Baïliche, M. T. Belaroussi, T. Mohamed, and H. Barthélemy, "Compact inductorless CMOS low-noise amplifier for reconfigurable radio," *Electron. Lett.*, vol. 50, no. 12, pp. 892–893, Jun. 2014, doi: 10.1049/el.2014.1031.

[49] A. Kumar and N. P. Pathak, "Varactor-tunable dual-band filtering low-noise amplifier," *Microw. Opt. Technol. Lett.*, vol. 60, no. 5, pp. 1118–1125, Apr. 2018, doi: 10.1002/mop.31117.

ANDRÉS FONTANA (Member, IEEE) received the Ph.D. degree in high-frequency electronics from the University of Limoges, Limoges, France, in 2022. He is currently a Post-Doctoral Researcher with the Advanced RF Technologies (ART) Group, Tyndall National Institute, Cork, Ireland. His research interests include RF active and passive devices and subsystems, monolithic microwave integrated circuit (MMIC) design, additive manufacturing, and heterogeneous integration technologies for wireless communication applications.

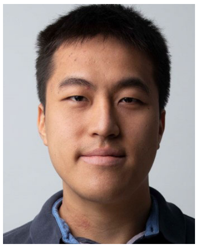

STEVEN MATTHEW CHENG (Graduate Student Member, IEEE) received the bachelor's degree in electronics and communications engineering and the master's degree in electrical engineering from the University of the Philippines Diliman, in 2015 and 2017, respectively. He is currently pursuing the Ph.D. degree in electrical and electronic engineering with University College Cork (UCC), Ireland. His current research interests include the design of low-noise amplifiers, microwave filters, reconfigurable RF front-ends, and co-integration of RF passive and active components.

DIMITRA PSYCHOGIOU (Senior Member, IEEE) received the Dipl.-Eng. degree in electrical and computer engineering from the University of Patras, Patras, Greece, in 2008, and the Ph.D. degree in electrical engineering from the Swiss Federal Institute of Technology (ETH), Zürich, Switzerland, in 2013. She is currently a Professor of electrical and electronic engineering with University College Cork (UCC) and the Head of the Advanced RF Technology Group, Tyndall National Institute, Cork, Ireland. Prior to joining UCC, she was a Senior Research Scientist with Purdue University, West Lafayette, IN, USA, and an Assistant Professor with the University of Colorado Boulder, Boulder, CO, USA. Her current research interests include RF design and characterization of reconfigurable microwave and millimeter-wave passive components, RF-MEMS, acoustic wave resonator-based filters, tunable filter synthesis, frequency-agile antennas, and additive manufacturing technologies for 3D antenna sub-systems. Her research has been presented in more than 250 scientific publications and received multiple awards, including the 2023 IEEE MTT-S Outstanding Young Engineer Award, the 2021 Roberto Sorrentino Prize, the SFI Research Professorship Award, the 2020 NSF CAREER Award, the 2020 URSI Young Scientist Award, and the Junior Faculty Outstanding Research Award from UC Boulder. She is a Senior Member of URSI and a member of the IEEE MTT-S Filters and Passive Components (MTT-5) and Microwave Control Materials and Devices (MTT-13) committees. She is also serving as the President for URSI Ireland, the Vice-Chair for MTT-13, and the Secretary for USNC-URSI Commission D. She is also an Associate Editor of the IEEE Microwave and Wireless Components Letters and the *International Journal of Microwave and Wireless Technologies* and is on the Technical Review Board of various IEEE and EuMA conferences. Previously, she was an Associate Editor of the *IET Microwaves, Antennas and Propagation*.